Pergamon
www.elsevier.com/locate/asr
Adv. Space Res. Vol. 29, No. 4, pp. 497–503, 2002

Printed in Great Britain
0273-1177/02 $22.00 + 0.00
PII: S0273-1177(01)00647-0

FIRST RESULTS FROM THE COSMIC DUST AGGREGATION EXPERIMENT CODAG

J. Blum[1], G. Wurm[2], T. Poppe[1], S. Kempf[3], and T. Kozasa[4]

[1]*Astrophysical Institute and University Observatory, Schillergässchen 2-3, 07745 Jena, Germany*
[2]*Laboratory for Atmospheric and Space Physics, University of Colorado, Campus Box 392, Boulder, CO 80309-0392, USA*
[3]*Max Planck Institute for Nuclear Physics, Saupfercheckweg 1, 69117 Heidelberg, Germany*
[4]*Division of Earth and Planetary Sciences, Graduate School of Science, Hokkaido University, Sapporo 060-0810, Japan*

ABSTRACT

The Cosmic Dust Aggregation Experiment (CODAG), an experimental simulation of the onset of planet formation, was successfully flown on STS-95 (October/November 1998) and on Maser 8 (May 1999). The main objective of the CODAG experiment was a direct observation of the Brownian motion-induced coagulation process of micron-sized dust particles. To overcome rapid sedimentation of the dust grains in the rarefied gas atmosphere, experiments were conducted in a long-duration microgravity environment. In the experiment, we observed that within several minutes the initially deagglomerated dust grains formed fractal dust aggregates due to their thermal motion and subsequent mutual collisions. The results from this experiment are the first experimental proof that the concept of pre-planetary dust coagulation is correct.

INTRODUCTION

For the formation of planetesimals, the km-sized precursors of planets, circumstellar dust grains need to agglomerate. In the initial phase, μm-sized dust particles collide due to their Brownian motion and stick to each other due to van der Waals forces (Weidenschilling and Cuzzi, 1993). The growth rate of the pre-planetary dust in this stage depends strongly on the structure of the dust aggregates, which is not self-consistently predictable. Monte Carlo simulations of Brownian motion-driven dust aggregation predict (1) quasi-monodisperse distributions of aggregate masses, (2) a relation between aggregate mass m and size s of

$$m \propto s^{D_f}, \tag{1}$$

with $D_f \approx 1.8$ being the so-called fractal dimension, and (3) a temporal behavior of the mean aggregate mass of $\bar{m} \propto t^z$, with $z \approx 2$ (Kempf et al., 1999). As a test of this model and for the determination of aggregate masses, sizes, and growth rates under pre-planetary nebula conditions (i.e. micron-sized dust grains of cosmically-relevant materials, ballistic collisions induced by Brownian motion in a rarefied gas), we developed the Cosmic Dust Aggregation Experiment CODAG (Keller et al., 1993, Huijser et al., 1997, Blum et al., 1999a,b). To accelerate the agglomeration process in the Brownian motion-determined growth phase, which takes several years in pre-planetary accretion disks, we performed the CODAG experiments with dust grain number densities of $\sim 10^{12}$ m^{-3}, several orders of magnitude higher than in the solar nebula. However, the physics of the coagulation process is unaffected by this; only the timescale of the growth process scales

inversely proportional to the particle number density, so that we can expect a considerable aggregate growth within a few minutes. To prevent coagulation by the overwhelming effect of sedimentation in Earth's gravity field, a microgravity environment is required. CODAG was flown as a Get Away Special payload on STS-95 in October/November 1998 and on-board the Maser 8 sounding rocket (MAterials Science Experiment Rocket) in May 1999.

THE CODAG EXPERIMENTS

Instrumentation

By means of a small pyrotechnical device, clouds of single, micron-sized dust particles were dispersed into rarefied gases (20% CO_2, 20% O_2, 40% H_2O, 20% N_2) of pressure $p = 0.5 - 2$ mbar and temperature $T = 300$ K. Due to the low gas pressure, a molecular gas flow around the dust grains was present. The particle motion close to the contact between two dust grains was ballistic, so that, even if the physical conditions are quite different (e.g. gas composition, number density of dust grains), the agglomeration process in the experiment closely resembles the one that occurred in the young Solar System. The dust grains' motion and the aggregates' structures were analyzed with a specially-developed stereo long-distance microscope with attached high-speed digital CCD cameras. The field of view of each of the two microscopes was 0.25×0.25 mm^2, with a spatial resolution of 1 μm, a focal depth of ~ 80 μm, and a temporal resolution of 5 msec. The CCD sensors were chosen such that each of its pixels covered an area of 1×1 μm^2. In addition to the direct microscopical observation of dust aggregates, both CODAG instruments were also equipped with light-scattering units for the analysis of the angular dependence of intensity and polarization of laser light scattered by the dust aggregates. More details of the CODAG experiments can be found in Blum et al. (1999a,b).

Dust Samples

As dust samples we used in the CODAG experiments (1) monodisperse SiO_2 spheres with radii $s_0 = 0.95$ μm and masses $m_0 = 7.2 \times 10^{-15}$ kg, (2) monodisperse SiO_2 spheres with radii $s_0 = 0.50$ μm and masses $m_0 = 1.0 \times 10^{-15}$ kg, and (3) micro-diamonds with radii in the range of $s_0 = 0.65 \ldots 0.95$ μm. SiO_2 resembles the cosmically-abundant material class of silicates in size and composition, whereas the micro-diamonds are used as analogs for the carbonaceous materials. Of particular interest for a comparison with computer simulations are the monodisperse SiO_2 spheres, because they match the idealized numerical cases almost perfectly and allow a direct comparison between calculated and observed dust aggregate structures.

General Observations

Due to unexpected compaction and dislocation of the dust sample during the launch of the Space Shuttle and the sounding rocket, the dust was not perfectly deagglomerated within the pyrotechnical device but reached the opposite wall of the experiment chamber in the form of several small dust clumps. Upon impact of these clumps, whose residuals were detected as white dust spots on the black chamber walls, the dust was then perfectly deagglomerated and formed several small cloudlets. We detected those cloudlets, which, due to electrostatic forces, slowly drifted through the experimental volume with typical velocities of $0.25 - 0.4$ mm sec^{-1}, by (1) short systematic variations of the background illumination in the microscope pictures, (2) the occurrence of dust aggregates in the field of view of the microscopes (see Figure 1) within short time intervals, intermitted by the absence of dust grains, and (3) systematic signal variations in the light scattering instrument.

The Motion of the Dust Grains

By means of the two long-distance microscopes, dust particles were imaged and these high-precision measurements of particle positions were used for a detailed analysis of the motion of the dust grains. With the previously measured gas-grain friction time τ_f for monomers (Blum et al., 1996), we showed that the measured aggregate motion is basically thermal (with very minor contributions of electrostatic forces and the residual acceleration of the spacecraft), so that the sole relevant driver for aggregate growth is Brownian motion (Blum et al., 2000). Previously unconsidered, we also detected dust aggregate rotation (Figure 2) which, following a first preliminary analysis, seems to be purely thermal on the shortest timescales, which is consistent with an equipartition of energy among all degrees of freedom.

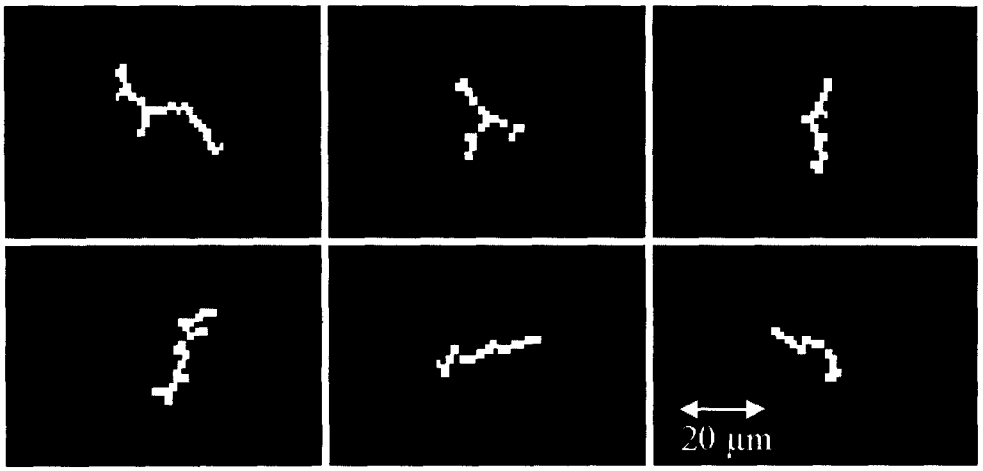

Fig. 1. Examples of dust agglomerates detected in the CODAG experiment.

RESULTS: AGGREGATE STRUCTURES

Figure 1 presents typical examples of the detected aggregates. The top row in Figure 1 shows aggregates consisting of SiO_2 spheres with $s_0 = 0.95$ μm, and the bottom row shows aggregates, which consist of micro-diamonds of approximately the same size. The analysis of the imaged aggregate structures shows that the mean ratio of their longest to shortest axis is $\rho \approx 3 - 4$, which is slightly higher than for aggregates grown in a turbulent rarefied gas (Wurm and Blum, 2000).

As the mass distribution of the experimental dust aggregates could not be matched with existing ballistic cluster-cluster aggregation (BCCA) models, we developed a new hierarchical aggregation code in which we implemented a restriction to the allowed values of the impact parameter. An excellent match between the experimental and the simulated internal mass distributions could be reached if the normalized impact parameter was restricted to $\psi > 0.65$ (Blum et al., 2000). Here, $\psi = 0$ denotes a central collision, and $\psi = 1$ is a grazing incidence between two dust aggregates in which these aggregates touch with their outermost tips. Figure 3 shows examples of the simulated aggregates whose appearance is very similar to the aggregates detected with CODAG. As is suggested by the visual appearance of the aggregates, their fractal dimensions are $D_f \ll 2$. We determined the fractal dimensions for the numerically-simulated aggregates with $\psi > 0.65$ by plotting the logarithm of the aggregate mass as a function of the logarithm of the radius of gyration. It turned out that the mass-size relation follows a power law (Eq. 1) with a slope of $D_f \approx 1.3$. Such low fractal dimensions were quite unexpected. Following a preliminary and qualitative analysis, we regard the aggregate rotation as being responsible for the elongated, highly asymmetric particle morphologies. A reasonably high rotation velocity can lead to non-central collisions, even if the linear motion of the dust aggregates indicates $\psi = 0$.

RESULTS: AGGREGATE GROWTH

A detailed analysis of the observed aggregate structures, utilizing their close similarity to the numerically simulated agglomerates, led to the determination of the aggregate masses. At this stage of the data analysis, we present results for the SiO_2 particles with $s_0 = 0.95$ μm. Due to the cloudlet structure of the dust distribution inside the experiment chamber, we could not directly measure the initial condition of the mass distribution function. To compensate for this, we performed a set of laboratory experiments with the flight hardware in which we treated the setup in the same way as in the Space Shuttle flight, including the simulation of launch vibrations. As in the spaceflight, we observed the formation of dust cloudlets upon dust injection and the subsequent sedimentation of the dust particles, during which we took long-distance microscope pictures. These experiments showed unambiguously that the deagglomeration of the dust was very efficient. The mean monomer number in the initially-present dust agglomerates was $\bar{\mu}(0) = 2 \pm 1$. In the STS-95 experiment presented here, we detected two dust cloudlets at $t = 55$ sec and $t = 100$ sec after

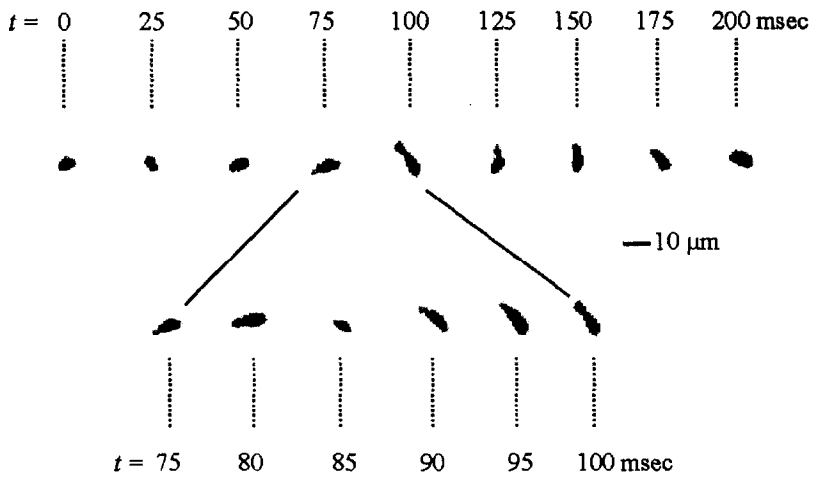

Fig. 2. High spatial- and temporal-resolution imaging reveals the Brownian rotation of dust agglomerates. This image sequence was taken during the Maser 8 sounding rocket flight.

dust injection. Both cloudlets had identical monomer number densities of $n_0 = 1 \times 10^{12}$ m^{-3} which allowed us to plot the measured aggregate masses of both clouds in one diagram. Figure 4 shows these data, where the open circles represent mass and time-of-occurrence of the individual agglomerates. Unambiguously, the mean aggregate mass increases with time.

Electrostatic Charges and Dipole Moments

To estimate the influence of electrostatic charges and dipole moments on the aggregation process, we deduced the maximum mean number of elementary charges on each monomer grain. The best-constrained upper limit for the charge-to-mass ratio of the dust grains can be derived under the assumption that the individual dust cloudlets expanded by electrostatic repulsion between the uniformly-charged dust grains. The above-mentioned drift of all dust grains through the experiment chamber can reasonably be explained only by the presence of a (very low) electrostatic charge of equal sign on the majority of the particles. An external electrical field, generated e.g. by charging of the chamber's non-conductive windows, would then be responsible for the systematic particle drift, and cumulative effects of the particle ensemble would tend to enhance the drift velocity and thus to equilibrate differences in drift velocity. Assuming the worst case of an initially point-like dust cloudlet, each monomer in the cloud cannot have more elementary charges than $q \leq \sqrt{\frac{\epsilon_0 m_0}{\tau_f e^2 n_0}\left(\frac{1}{t}\right)}$ to reach a measured monomer number density (see below) of $n_0 = 1 \times 10^{12}$ m^{-3} within the time t. Here, ϵ_0 and e are the dielectric constant and the elementary charge, respectively. For the typical times of the dust cloud observation of $t = 100$ s, we get an upper limit of $q \approx 2-3$ elementary charges. With an average (net) charge of 3 elementary charges per monomer, we can derive that the electrical field strength responsible for the cloudlet drift has to be of the order of $E = 1000$ V m^{-1}. With this canonical value, we can estimate the maximum dipole moment of the dust aggregates: our analysis showed that aggregates, although having highly elongated structures (see Figure 1), are not aligned with respect to the electrical field vector. This can only be the case if the energy of the electrical dipoles with mean dipole moment p in the electrical field is not exceeding the thermal energy, i.e. $p < \frac{kT}{E} \approx 4 \times 10^{-24}$ Cm $\approx 3\ e \cdot 10\ \mu$m, with k being the Boltzmann constant. As the mean aggregate length is of the order of 10 μm, the particle clusters cannot consist of highly charged monomers with alternating sign, even if the overall charge budget might be low. For $q \leq 3\ e = 5 \times 10^{-19}$ C and $p \leq 4 \times 10^{-24}$ Cm, we can compare the electrostatic potentials with the thermal energy of the dust grains, $E_{\rm th} \approx kT = 4 \times 10^{-21}$ J. The electrostatic repulsion energy of two touching grains is given by $E_{\rm q} = \frac{1}{4\pi\epsilon_0}\frac{q^2}{2s_0} \leq 1 \times 10^{-21}$ J for $s_0 = 1\ \mu$m; the energy of a charged particle in the electrostatic dipole field of a 10 μm long dust aggregate can be approximated by $E_{\rm p} = \frac{1}{4\pi\epsilon_0}\frac{pq}{r^2} \leq 7 \times 10^{-22}$

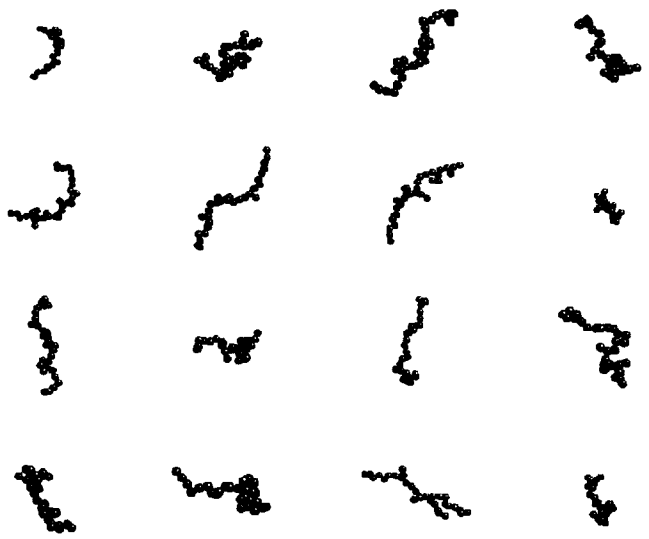

Fig. 3. Examples of the simulated agglomerates with $\psi > 0.65$.

J, when we assume that the charged dust grain is $r = 5$ μm away from the center of the (linear) aggregate. Hence, any electrostatic interaction between approaching aggregates does not possess sufficient energy to cause a mutual alignment between the aggregates and can, thus, not be responsible for the formation of the observed elongated structures. As the electrostatic energy of each pair of colliding, slightly-charged grains is always lower than their thermal energy, this experiment represents a valid simulation of the pre-planetary aggregation process.

MODELING THE AGGREGATE GROWTH

Under the very well justified assumption of quasi-monodisperse growth (see below), we modeled the aggregation of dust grains using the mass-accumulation equation

$$\frac{\partial \bar{\mu}(t)}{\partial t} = \frac{\bar{\mu}^{\beta}}{t_1}, \tag{2}$$

in which $\bar{\mu}(t)$, β, and t_1 are the mean aggregate mass in units of the monomer mass m_0 at the time t, the exponent describing the mass dependence of the product of collision cross section σ_c and collision velocity v_c, i.e. $\sigma_c \cdot v_c \propto \bar{\mu}^{\beta}$, and the monomer collision time $t_1 = (n_0 \sigma_{11} v_{11})^{-1}$, respectively. Here, $n_0 = 1 \cdot 10^{12}$ m^{-3}, $\sigma_{11} = 1.2 \cdot 10^{-5}$ m^2, and $v_{11} = 1.7 \cdot 10^{-3}$ m sec^{-1} are the monomer number density, the monomer-monomer collision cross section, and the mean relative thermal velocity between monomers. If we allow for an uncertainty of a factor 2 in the determination of the mean number density, we get $t_1 = 50^{+50}_{-25}$ sec.

The solution to the mass-accumulation equation (Eq. 2) reads

$$\bar{\mu} = \left(\bar{\mu}(0)^{1/z} + \frac{t}{z t_1} \right)^{z}, \tag{3}$$

with z being related to β by $\frac{z-1}{z} \equiv \beta$ (see Meakin, 1991 for a detailed overview on aggregation kinetics). Three curves in Figure 4 show these mass-growth functions for $t_1 = 50$ sec, $\bar{\mu}(0) = 3$, $z = -8$ (dotted line), $t_1 = 25$ sec, $\bar{\mu}(0) = 2$, $z = 8$ (solid line), and $t_1 = 33$ sec, $\bar{\mu}(0) = 2$, $z = \infty$ (exponential growth, dash-dotted line). For all sensible parameter combinations, the absolute value of z is rather large. This constrains, however, the exponent β to $\beta = \frac{7}{8} \ldots \frac{9}{8}$. For aggregates with $\sigma_c \propto s^2 \propto m^{\frac{2}{D_f}}$ with $D_f = 1.3$ and thermal motion ($v_r \propto m^{-\frac{1}{2}}$), we expect $\beta = \frac{2}{D_f} - \frac{1}{2} \approx 1.04$ (Meakin, 1991). This means that a near-exponential growth of the mean aggregate mass is expected and can be explained by the observed aggregate masses.

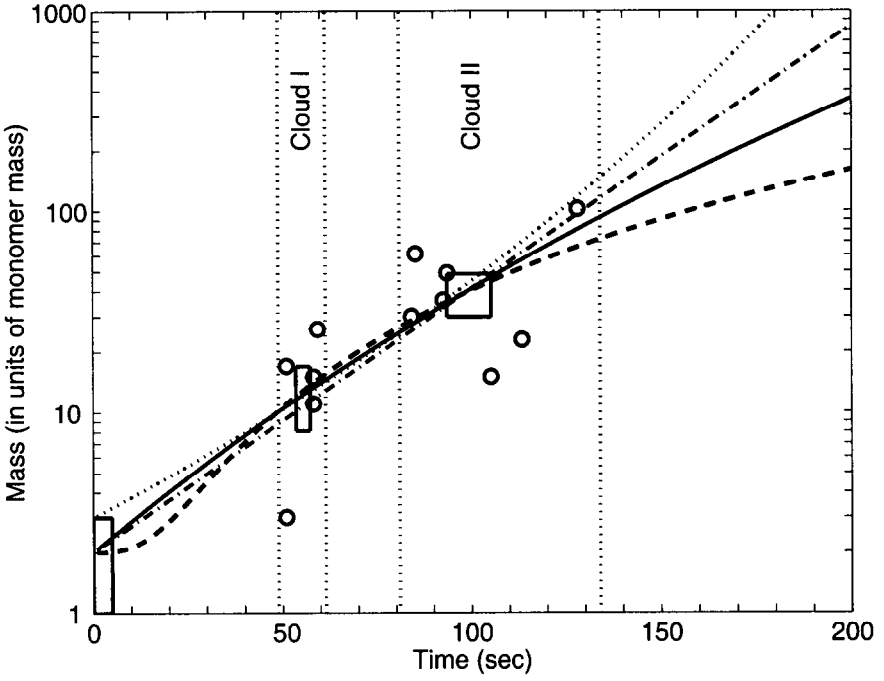

Fig. 4. Comparison of measured and calculated aggregate masses. The open circles the open boxes denote the 1σ uncertainty of the mean aggregate mass and time-of-occurrence for both dust clouds as well as for the initial condition. The four curves are model calculations for faster-than-exponential growth (dotted curve), exponential growth (dash-dotted curve), power-law growth with exponent 8 (solid curve), and power-law growth with exponent 2 (dashed curve).

However, the above growth model might be an oversimplification of reality. Numerical simulations of the Brownian motion-caused aggregation by Kempf et al. (1999) predict a somewhat slower mass growth with $z \approx 2$ (but keep in mind that this model predicts $D_f \approx 1.8$), which does not follow the solution (Eq. 3) to the quasi-monodisperse growth equation. As the local slope of the mass growth in Figure 4 between $t = 50$ sec and $t = 100$ sec is approximately 2, we cannot exclude any model that predicts $z = 2$ with a somewhat different (and faster) transition between the initial condition $\bar{\mu}(0)$ and the asymptotic power law (see dashed line in Figure 4).

The cumulative mass spectrum of the SiO_2 aggregates in the CODAG experiment was derived by extrapolation of the measured aggregate masses to a common time basis of $t = 100$ sec. For this, we used a power law $\mu(t) \propto t^2$ which is a valid approximation to the local mass-time behavior between 50 and 100 sec. The so-derived cumulative mass spectrum represents a power law with an exponent $2 - \lambda = 1.8$. Thus, the mass spectrum reads $n(\mu)\mathrm{d}\mu \propto \mu^{-\lambda}\mathrm{d}\mu$, with $\lambda = 0.2$. To a good approximation, this mass spectrum can be considered as quasi-monodisperse.

CONCLUSION AND FUTURE WORK

With the results of the CODAG microgravity experiments, we have shown that quasi-ballistic Brownian motion-driven dust aggregation in the free molecular flow regime is a fast and efficient way for the formation of larger dust aggregates in the solar nebula, which leads to unexpected asymmetric aggregate structures with $D_f \approx 1.3$. With our data and at this stage of the aggregation modeling, we cannot exclude prior growth models which predict $\bar{\mu}(t) \propto t^2$, but the CODAG results indicate a somewhat faster growth of $\bar{\mu}(t) \propto \exp(t)$. However, the difference between the various growth models is relatively unimportant for the pre-planetesimal dust aggregation, because Brownian motion-driven aggregation will be superseded by the aggregation stemming from differential sedimentation of the dust grains, when the dust aggregates consist

of $\bar{\mu} \approx 100$ micron-sized monomer grains. As shown in Figure 4, even the most extreme predictions for the growth timescales of such aggregates differ by less than a factor of two. In any case, new numerical simulations, which include the hitherto neglected effects of thermal aggregate rotation, are needed. Such new models are currently planned by the authors of this article.

ACKNOWLEDGEMENTS

This work was supported by the German Space Agency DLR and by the European Space Agency ESA.

REFERENCES

Blum, J., M. Schnaiter, G. Wurm, and M. Rott, The De-Agglomeration and Dispersion of Small Dust Particles - Principles and Applications, *Rev. Sci. Instrum.*, **67**, 589-595, 1996.

Blum, J. et al., The Cosmic Dust Aggregation Experiment CODAG, *Measurement Science & Technology*, **10**, 836-844, 1999a.

Blum, J., G. Wurm, and T. Poppe, The CODAG Sounding Rocket Experiment to Study Aggregation of Thermally Diffusing Dust Particles, *Adv. Space Res.*, **23**, 1267-1270, 1999b.

Blum, J. et al., On Growth and Form of Planetary Seedlings, *Phys. Rev. Lett.*, **85**, 2426-2429, 2000.

Huijser, R.H. et al., CODAG-1: Development of a Sounding Rocket Module to Study Cosmic Dust Agglomeration, *Proc. 13th ESA Symp. on European Rocket and Balloon Programmes and Related Research*, **ESA SP-397**, 77-83, 1997.

Keller, H.U. et al., CODAG - Dust Agglomeration Experiment in Micro Gravity, *Adv. Space Res.*, **13**, 73-76, 1993.

Kempf, S., S. Pfalzner, and Th. Henning, N-particle-Simulations of Dust Growth, *Icarus*, **141**, 388-398, 1999.

Meakin, P., Fractal Aggregates in Geophysics, *Review of Geophysics*, **29**, 317-354, 1991.

Weidenschilling, S.J., and J.N. Cuzzi, Formation of Planetesimals in the Solar Nebula, in Protostars and Planets III, eds. E.H. Levy, J.I. Lunine, pp. 1031-1060, University of Arizona Press, Tucson and London, 1993.

Wurm, G., and J. Blum, An Experimental Study on the Structure of Cosmic Dust Aggregates and their Alignment by Motion Relative to Gas, *Astrophys. J.*, **529**, L57-L60, 2000.